Tight-binding description of graphene

S. Reich, J. Maultzsch, and C. Thomsen
Institut für Festkörperphysik, Technische Universität Berlin, Hardenbergstrasse 36, 10623 Berlin, Germany

P. Ordejón
Institut de Ciència de Materials de Barcelona (CSIC), Campus de la U.A.B. E-08193 Bellaterra, Barcelona, Spain

(Received 22 April 2002; revised manuscript received 10 May 2002; published 19 July 2002)

We investigate the tight-binding approximation for the dispersion of the π and π^* electronic bands in graphene and carbon nanotubes. The nearest-neighbor tight-binding approximation with a fixed γ_0 applies only to a very limited range of wave vectors. We derive an analytic expression for the tight-binding dispersion including up to third-nearest neighbors. Interaction with more distant neighbors qualitatively improves the tight-binding picture, as we show for graphene and three selected carbon nanotubes.

DOI: 10.1103/PhysRevB.66.035412 PACS number(s): 71.20.Tx, 73.61.Wp, 78.66.Tr

The band structure of carbon nanotubes is widely modeled by a zone-folding approximation of the graphene π and $\pi^\star$ electronic states as obtained from a tight-binding Hamiltonian.[1–5] The large benefit of this method is the very simple formula for the nanotube electronic bands. While the tight-binding picture provides qualitative insight into the one-dimensional nanotube band structure, it is more and more being used for quantitative comparisons as well. For instance, attempts to assign diameters and chiralities of carbon nanotubes based on optical absorption and Raman data rely heavily on the assumed transition energies.[2,6] Differences between the zone-folding, tight-binding π-orbital description and experiment, as observed, e.g., in scanning tunneling measurements, are usually ascribed to ''curvature effects.''[1] However, the common π-orbital tight-binding approach for the nanotube band structure involves two approximations: (i) zone folding, which neglects the curvature of the wall; and (ii) the tight-binding approximation to the graphene bands including only first-neighbor interaction. Whereas the first point received some attention in the literature,[7–9] the second approximation is usually assumed to be sufficient.

In this paper we compare the tight-binding approximation of the graphene π orbitals to first-principles calculations. We show that the nearest-neighbor tight-binding Hamiltonian does not accurately reproduce the π and π^* graphene bands over a sufficiently large range of the Brillouin zone. We derive an improved tight-binding electronic dispersion by including up to third-nearest-neighbor interaction and overlap. The formula for the electronic states we present may readily be used, e.g., in combination with zone folding to obtain the band structure of nanotubes.

The first tight-binding description of graphene was given by Wallace in 1947.[10] He considered nearest- and next-nearest-neighbor interaction for the graphene p_z orbitals, but neglected the overlap between wave functions centered at different atoms. The other—nowadays better known—tight-binding approximation was nicely described by Saito *et al.*[4] It considers the nonfinite overlap between the basis functions, but includes only interactions between nearest neighbors within the graphene sheet. To study the different levels of approximation we start from the most general form of the secular equation, the tight-binding Hamiltonian H, and the overlap matrix S,[4]

$$\begin{vmatrix} H_{AA}(\boldsymbol{k})-E(\boldsymbol{k})S_{AA}(\boldsymbol{k}) & H_{AB}(\boldsymbol{k})-E(\boldsymbol{k})S_{AB}(\boldsymbol{k}) \\ H^*_{AB}(\boldsymbol{k})-E(\boldsymbol{k})S^*_{AB}(\boldsymbol{k}) & H_{AA}(\boldsymbol{k})-E(\boldsymbol{k})S_{AA}(\boldsymbol{k}) \end{vmatrix} = 0, \quad (1)$$

where $E(\boldsymbol{k})$ are the electronic eigenvalues. We used the equivalence of the A and B carbon atoms in the graphene sheet. The solution to Eq. (1) is

$$E(\boldsymbol{k})^{\pm} = \frac{-(-2E_0+E_1) \pm \sqrt{(-2E_0+E_1)^2-4E_2E_3}}{2E_3}, \quad (2)$$

with

$$E_0 = H_{AA}S_{AA}, \quad E_1 = S_{AB}H^*_{AB}+H_{AB}S^*_{AB}$$

$$E_2 = H^2_{AA}-H_{AB}H^*_{AB} \quad E_3 = S^2_{AA}-S_{AB}S^*_{AB}. \quad (3)$$

To outline the procedure of setting up the Hamiltonian and overlap matrix let us briefly derive the nearest-neighbor tight-binding dispersion (for a more complete description see Ref. 4). For an atom A_0 as shown in Fig. 1 the nearest neigh-

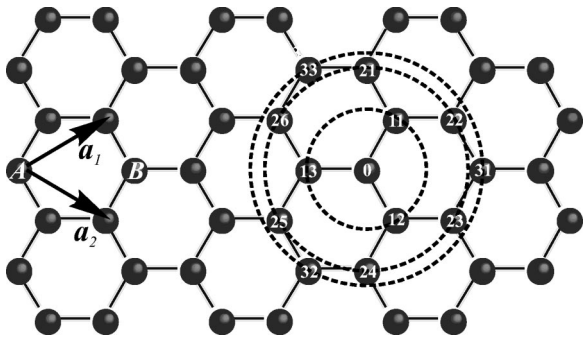

FIG. 1. Graphene hexagonal lattice. $\boldsymbol{a}_1$ and $\boldsymbol{a}_2$ are the unit-cell vectors of graphene with a lattice constant $a=2.461$ Å. The unit cell contains two carbon atoms A and B belonging to the two sublattices. An atom A_0 has three nearest neighbors B_{1i}, six next-nearest neighbors A_{2i}, and three second-nearest neighbors B_{3i}.

bors are B_{11}, B_{12}, and B_{13}, all of which belong to the other graphene sublattice; thus for nearest-neighbor interaction

$$H_{AA}=\frac{1}{N}\sum_{\boldsymbol{R}_A}\sum_{\boldsymbol{R}_{A'}} e^{i\boldsymbol{k}(\boldsymbol{R}_{A'}-\boldsymbol{R}_A)}\langle\varphi_A(\boldsymbol{r}-\boldsymbol{R}_A)|H|\varphi_A(\boldsymbol{r}-\boldsymbol{R}_{A'})\rangle$$

$$=\frac{1}{N}\sum_{\boldsymbol{R}_A}\langle\varphi_A(\boldsymbol{r}-\boldsymbol{R}_A)|H|\varphi_A(\boldsymbol{r}-\boldsymbol{R}_A)\rangle=\varepsilon_{2p}, \qquad (4)$$

where N is the number of unit cells in the crystal, $\boldsymbol{R}_A$ and $\boldsymbol{R}_{A'}$ are the positions of atom A and A', respectively, and φ_A denote the p_z atomic wave functions forming the basis for the crystal Bloch functions. The overlap matrix element $S_{AA}=1$, since we assume the atomic wave functions to be normalized $[\langle\varphi_A(\boldsymbol{r}-\boldsymbol{R}_A)|\varphi_A(\boldsymbol{r}-\boldsymbol{R}_A)\rangle=1]$. To find H_{AB} within the nearest-neighbor approximation, we simply sum over the three nearest neighbors shown in Fig. 1:

$$H_{AB}=\frac{1}{N}\sum_{\boldsymbol{R}_A}\sum_{\boldsymbol{R}_B} e^{i\boldsymbol{k}(\boldsymbol{R}_B-\boldsymbol{R}_A)}\langle\varphi_A(\boldsymbol{r}-\boldsymbol{R}_A)|H|\varphi_B(\boldsymbol{r}-\boldsymbol{R}_B)\rangle$$

$$=\gamma_0(e^{i\boldsymbol{k}\boldsymbol{R}_{11}}+e^{i\boldsymbol{k}\boldsymbol{R}_{12}}+e^{i\boldsymbol{k}\boldsymbol{R}_{13}})$$

with

$$\gamma_0=\langle\varphi_A(\boldsymbol{r}-\boldsymbol{R}_A)|H|\varphi_B(\boldsymbol{r}-\boldsymbol{R}_A-\boldsymbol{R}_{1i})\rangle \quad (i=1,2,3),$$

the same treatment yields the overlap matrix element

$$S_{AB}=s_0(e^{i\boldsymbol{k}\boldsymbol{R}_{11}}+e^{i\boldsymbol{k}\boldsymbol{R}_{12}}+e^{i\boldsymbol{k}\boldsymbol{R}_{13}})$$

with

$$s_0=\langle\varphi_A(\boldsymbol{r}-\boldsymbol{R}_A)|\varphi_B(\boldsymbol{r}-\boldsymbol{R}_A-\boldsymbol{R}_{1i})\rangle \quad (i=1,2,3),$$

where $\boldsymbol{R}_{1i}$ is the vector pointing from atom A_0 to atoms B_{1i} in Fig. 1. Now we insert the Hamiltonian and overlap matrix elements into Eqs. (3) and (2). We define the function

$$f(\boldsymbol{k})=3+u(\boldsymbol{k})$$

$$=3+2\cos\boldsymbol{k}\cdot\boldsymbol{a}_1+2\cos\boldsymbol{k}\cdot\boldsymbol{a}_2+2\cos\boldsymbol{k}\cdot(\boldsymbol{a}_1-\boldsymbol{a}_2)$$

$$=3+2\cos 2\pi a k_1+2\cos 2\pi a k_2+2\cos 2\pi a(k_1-k_2), \qquad (5)$$

where $k_i=\boldsymbol{k}\cdot\boldsymbol{a}_i/2\pi$ are the components of a wave vector $\boldsymbol{k}$ in units of the reciprocal graphene lattice vectors $\boldsymbol{k}_1$ and $\boldsymbol{k}_2$, and obtain the well-known result[4]

$$E^{\pm}(\boldsymbol{k})=\frac{\varepsilon_{2p}\mp\gamma_0\sqrt{f(\boldsymbol{k})}}{1\mp s_0\sqrt{f(\boldsymbol{k})}}. \qquad (6)$$

The three parameters ε_{2p}, γ_0, and s_0 are found by fitting experimental or first-principles data. The most common practice is to adjust the tight-binding dispersion to a correct description of the π bands at the K point. This yields $\varepsilon_{2p}=0$ eV, γ_0 between -2.5 and -3 eV, and s_0 below 0.1. Since s_0 is small, it is usually neglected. The nearest-neighbor Hamiltonian is able to produce bands which are not symmetric with respect to the Fermi level, but only if the overlap s_0 is nonzero.

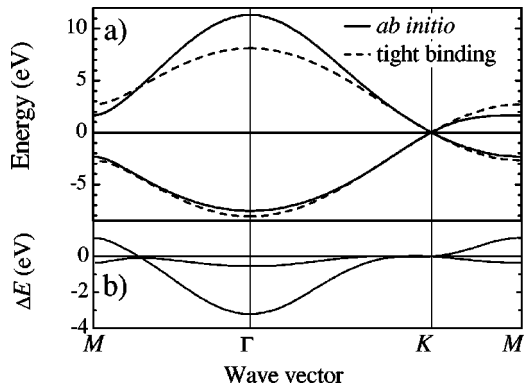

FIG. 2. *Ab initio* and nearest-neighbor tight-binding dispersions of graphene. (a) The converged *ab initio* calculation of the graphene π and π^* electronic bands is shown by the full lines. The dashed lines represent the tight-binding dispersion of Eq. (6) with $s_0=0$ and $\gamma_0=-2.7$ eV. (b) Difference ΔE between the *ab initio* and tight-binding band structures.

The nearest-neighbor tight-binding description of graphene was originally developed to study the low-energy properties of graphite, i.e., the focus was not on the in-plane dispersion, but rather on the coupling between the graphene sheets. As the interest rose in nanotubes, Eq. (6) (with $s_0=0$) was adopted for the electronic band structure throughout the entire Brillouin zone. In Fig. 2(a) we show an *ab initio* calculation of the graphene π and π^* bands (full lines) and the tight-binding dispersion [Eq. (6)], neglecting the overlap matrix (dashed lines) and in Fig. 2(b) the difference between the two calculations. An interaction parameter $\gamma_0=-2.7$ eV was used, a typical value which best reproduced the slopes of the valence and conduction bands at the K point from the first-principles calculations. Our *ab initio* calculations were performed with the SIESTA code[11,12] using pseudopotentials[13] and the Perdew-Zunger parametrization[14] of the local-density approximation. An energy cutoff of 270 Ry was taken for real space integrations and a $40\times40\times1$ Monkhorst-Pack grid[15] in reciprocal space. The valence electrons were expanded in a basis of numerical pseudoatomic orbitals.[16,17] The converged band structure in Fig. 2 was obtained with a double-ζ, singly polarized basis set. The extension of the s orbitals was 5.12 a.u.$=2.71$ Å and of the p and d orbitals 6.25 a.u.$=3.31$ Å.[16] A further increase of the cutoff radii affected the electronic energies by less than 5 meV. We obtained a graphene lattice constant 2.468 Å; the binding energy and elastic constants agreed well with plane wave calculations and experiment.[18] For comparison we calculated the band structure of graphite and found good agreement with plane-wave pseudopotential calculations.[19,20]

In general the agreement between first-principles and the tight-binding band structure is rather poor; good agreement is only obtained very close to the K point of Brillouin zone, i.e., for the wave vectors used to determine γ_0. Even in the range of the visible transitions the electronic energies deviate by some 100 meV.

The benefit of the SIESTA method for the present discussion is that the self-consistent Hamiltonian is of a tight-binding type.[11,12] We can thus directly compare the level of

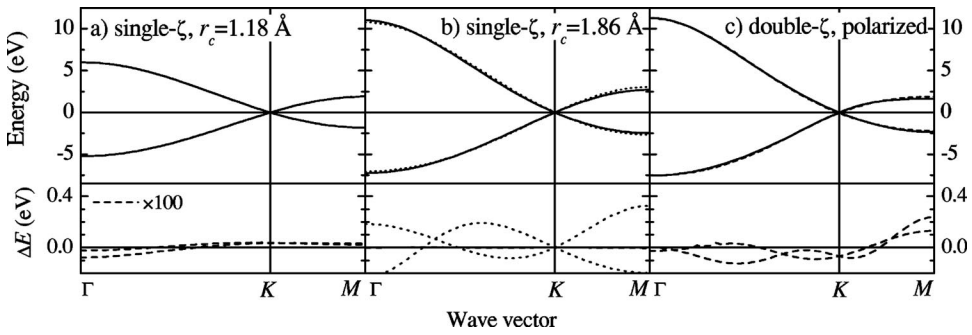

FIG. 3. (a) Top: first-principles band structure with a single-ζ basis set and $r_c=1.18$ Å. The nearest-neighbor tight-binding band structure [Eq. (6)] with $\gamma_0=-1.86$ eV and $s_0=0.02$ coincides with the first-principles result. Bottom: difference ΔE between the first-principles and nearest-neighbor tight-binding band structures. (b) Top, full lines: first-principles result with a single-ζ basis set and $r_c=1.86$ Å; dotted lines: nearest-neighbor tight-binding band structure [Eq. (6)] with $\gamma_0=-2.84$ eV and $s_0=0.070$; the third-nearest neighbor tight-binding band structure coincides with the first-principles result shown by the full lines ($\varepsilon_{2p}=-0.36$ eV, $\gamma_0=-2.78$ eV, $\gamma_1=-0.12$ eV, $\gamma_2=-0.068$ eV, $s_0=0.106$, $s_1=0.001$, and $s_2=0.003$). Bottom, dotted line: difference between the first-principles and the nearest-neighbor tight-binding band structure shown in the top panel. For the third-nearest neighbor tight-binding approximation the differences are not seen on the chosen energy scale. (c) Top: converged *ab initio* (full lines) and third-neighbor tight-binding (dashed) band structures; see Table I for the tight-binding parameters ($M\Gamma KM$). Bottom: difference between the two band structures above.

approximation (basis set completeness and extension) in an *ab initio* calculation to the empirical tight-binding Hamiltonian. For the first-principles band structure in Fig. 2(a) we used a basis set that (i) contained two independent radial functions to describe the *p* orbitals, and included a shell of polarizing *d* orbitals (double-ζ plus polarization basis set[16]), and (ii) had a radial cutoff of 3.31 Å, i.e., atoms as distant as 6.62 Å have a nonfinite overlap and interaction (corresponding to the ninth distant neighbor). To mimic the empirical approximation by the first-principles calculation we calculated the band structure for a simple basis (single-ζ) with a cutoff radius of 1.18 Å, which includes only the interaction with the nearest neighbors (see Fig. 1). The result is shown in Fig. 3(a). The differences between the single-ζ nearest-neighbor band structure and the converged result in Fig. 2(a) are obvious: The separation of the valence and conduction band is reduced, most strongly at the Γ point; also the asymmetry of the bonding and antibonding band is much smaller. As expected, the dispersion in Fig. 3(a) is perfectly reproduced by the nearest-neighbor tight-binding formula in Eq. (6), since the *ab initio* calculation with that basis set takes precisely that form. The tight-binding parameters we obtain are $\gamma_0=-1.86$ eV and $s_0=0.02$. The differences between the *ab initio* calculation and Eq. (6) with these parameters is smaller than 10^{-3} eV, as shown in the bottom of Fig. 3(a), and is due to numerical inaccuracies in the *ab initio* calculation.

We now increased the extension of the basis wave function to $r_c=1.86$ Å, while still using a simple basis set and obtained the band structure in Fig. 3(b) (full lines, top panel). At the Γ point the agreement between this calculation and the converged result is already quite satisfactory (2%); the *M* point energy of the conduction band is, however, overestimated by 55%. The best fit of the tight-binding expression [Eq. (6)] to the first-principles band structure is shown by the dotted lines in Fig. 3(b). The dotted line in the bottom panel represents the difference between the *ab initio* and empirical results, which is on the order of 100 meV for most points of the Brillouin zone. The interaction with the more distant neighbors can thus no longer be neglected.

Wallace in his tight-binding study already considered second-nearest-neighbor interaction, although at the cost of neglecting the overlap matrix.[10] An extension of the tight-binding interaction radius, however, has to include the second as well as the third-nearest neighbors, since the distance $|\boldsymbol{R}_{2i}|=2.461$ Å is very close to $|\boldsymbol{R}_{3i}|=2.842$ Å. To find the third-nearest-neighbor tight-binding dispersion we proceed exactly as outlined above. The sum over $\boldsymbol{R}_{A'}$ in H_{AA} and S_{AA} (H_{AB} and S_{AB}) now additionally include $\boldsymbol{R}_{A'}=\boldsymbol{R}_A+\boldsymbol{R}_{2i}$ ($\boldsymbol{R}_{Bi}=\boldsymbol{R}_A+\boldsymbol{R}_{3i}$). The E_i's in Eq. (3) are then given by

$$E_0=[\varepsilon_{2p}+\gamma_1 u(\boldsymbol{k})][1+s_1 u(\boldsymbol{k})], \tag{7}$$

$$E_1=2s_0\gamma_0 f(\boldsymbol{k})+(s_0\gamma_2+s_2\gamma_0)g(\boldsymbol{k})+2s_2\gamma_2 f(2\boldsymbol{k}), \tag{8}$$

$$E_2=[\varepsilon_{2p}+\gamma_1 u(\boldsymbol{k})]^2-\gamma_0^2 f(\boldsymbol{k})-\gamma_0\gamma_2 g(\boldsymbol{k})-\gamma_2^2 f(2\boldsymbol{k}), \tag{9}$$

$$E_3=[1+s_1 u(\boldsymbol{k})]^2-s_0^2 f(\boldsymbol{k})-s_0 s_2 g(\boldsymbol{k})-s_2^2 f(2\boldsymbol{k}), \tag{10}$$

$$g(\boldsymbol{k})=2u(\boldsymbol{k})+u(2k_1-k_2,k_1-2k_2). \tag{11}$$

$f(\boldsymbol{k})$ and $u(\boldsymbol{k})$ were defined in Eq. (5). γ_1 and γ_2 are the interaction energies with the second and third neighbors, and s_1 and s_2 are the corresponding overlaps. Inserting E_0 to E_3 into Eq. (2) yields the tight-binding electronic dispersion in the third-nearest-neighbor approximation. We thus included the same number of neighbors for the first-principles and tight-binding Hamiltonians. With the tight-binding parameters as given in the caption of Fig. 3 the agreement between the electronic energies is again very good, better than 10^{-2} eV. This difference is now partially due to numerical inaccuracies of the *ab initio* calculation, and to difficulties of the fitting procedure when the number of parameters is large.

The third-nearest-neighbor tight-binding approximation is not yet sufficient to correctly describe the converged *ab initio* calculations, since they needed a larger basis set and a

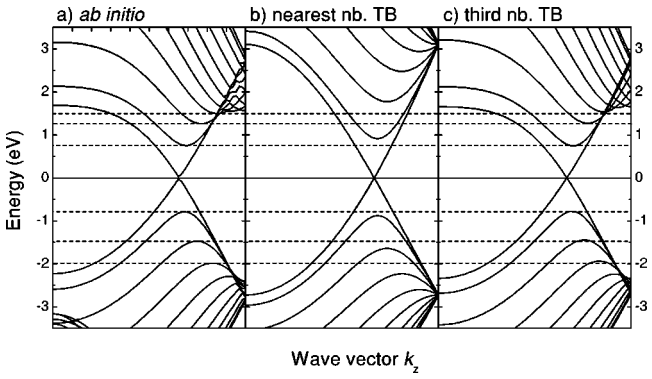

FIG. 4. Band structure of a (10,10) armchair nanotube. (a) *Ab initio* calculation. (b) Nearest-neighbor tight-binding calculation with $\gamma_0 = -2.7$ eV. (c) Third-nearest-neighbor tight-binding calculation with parameters obtained from a fit to the optical energy range; see Table I. The dashed lines denote *ab initio* calculated energies of the singularities in the density of states.

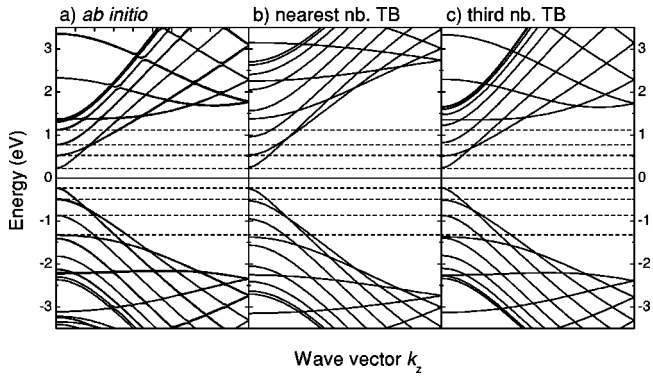

FIG. 5. Band structure of a (19,0) zigzag nanotube. (a) *Ab initio* calculation. (b) Nearest-neighbor tight-binding calculation with $\gamma_0 = -2.7$ eV. (c) Third-nearest-neighbor tight-binding calculation with parameters obtained from a fit to the optical energy range; see Table I. The dashed lines denote *ab initio* calculated energies of the singularities in the density of states.

higher cutoff radius. Nevertheless, we can quite accurately reproduce the first-principles results by considering only third-nearest neighbors. Figure 3(c) again shows the converged *ab initio* π band structure (top panel, full lines) together with the third-neighbor tight-binding approximation (dashed lines). The γ_i's and s_i's used for the tight-binding dispersion are listed in Table I ($M\Gamma KM$); at this point they should be considered fitting parameters rather than as having strict physical meanings. The difference between the *ab initio* and the empirical band structure is better than 250 meV along the high-symmetry lines, also see Fig. 3(c), bottom panel. For the optical range (transition energies <4 eV) we found an even better agreement (4 meV), with a slightly different set of parameters as given in Table I.

The third-neighbor approximation does not only yield a better fitting result along a given high-symmetry line than the nearest-neighbor approximation. Instead a set of tight-binding parameters found, e.g., from the optical energy range, gives reliable energies at low-symmetry k as well. To demonstrate this we show how the zone-folding band structure of carbon nanotubes improves by including more distant neighbors in the tight-binding Hamiltonian.

To obtain the band structure of a nanotube within zone folding we restrict the $\boldsymbol{k}$ vectors to the allowed wave vectors of the tube. The Γ point of an (n_1,n_2) nanotube is in terms of the graphene reciprocal lattice vectors given by[21]

$$\boldsymbol{k}_\Gamma(m) = m\left(\frac{2n_1+n_2}{qn\mathcal{R}}\boldsymbol{k}_1 + \frac{2n_2+n_1}{qn\mathcal{R}}\boldsymbol{k}_2\right), \tag{12}$$

where n is the highest common divisor of n_1 and n_2, $\mathcal{R}=3$ if $(n_1-n_2)/3n$ is an integer and $\mathcal{R}=1$ otherwise, $q=2(n_1^2+n_1n_2+n_2^2)/n\mathcal{R}$, and m is an integer running from $-q/2$ to $q/2-1$. The one-dimensional nanotube Brillouin zone is given by the wave vectors running from $\boldsymbol{k}_\Gamma(m)$ to $\boldsymbol{k}_\Gamma(m)+\boldsymbol{k}_z$ $(-q/2 \leqslant m \leqslant q/2-1)$, with

$$\boldsymbol{k}_z = -\frac{n_2}{q}\boldsymbol{k}_1 + \frac{n_1}{q}\boldsymbol{k}_2. \tag{13}$$

As a first example we consider a (10,10) armchair tube. In this tube curvature, effects are negligible since the diameter $d=1.44$ nm and the chiral angle $\Theta=30°$ are large.[7,8] Figure 4(a) shows the *ab initio* band structure of the (10,10) nanotube. The nearest-neighbor tight-binding dispersion in Fig. 4(b) correctly predicts the first optical transition energy, whereas the higher transition energies are strongly overestimated. The states at the center and the boundary of the Brillouin zone are incorrectly described by this simple approximation. In contrast, the agreement between the *ab initio* and the third-nearest-neighbor tight binding is excellent. The shape of the electronic dispersion as well as the absolute energies are very well described by the improved tight-binding approximation. In particular, the second singularity in the optical absorption probability is at an energy of 2.73 eV (453 nm) both from the *ab initio* and third-order tight-binding band structures, whereas the nearest-neighbor approximation perdicted a transition energy in the far UV (3.4 eV).

TABLE I. Tight-binding parameters. $M\Gamma KM$: fit to the *ab initio* energies for all k along the high-symmetry lines. optical: only the k yielding optical transitions with an energy <4 eV were included in the fit. ΔE_{max} (ΔE_{max} opt.) is the maximal deviation of the tight-binding from the *ab-initio* results for all k (only the optical range).

	ε_{2p} (eV)	γ_0 (eV)	s_0	γ_1 (eV)	s_1	γ_2 (eV)	s_2	ΔE_{max} (eV)	ΔE_{max} opt. (eV)
$M\Gamma KM$	−0.28	−2.97	0.073	−0.073	0.018	−0.33	0.026	0.25	0.25
optical	−2.03	−2.79	0.30	−0.68	0.046	−0.30	0.039	1.37	0.004

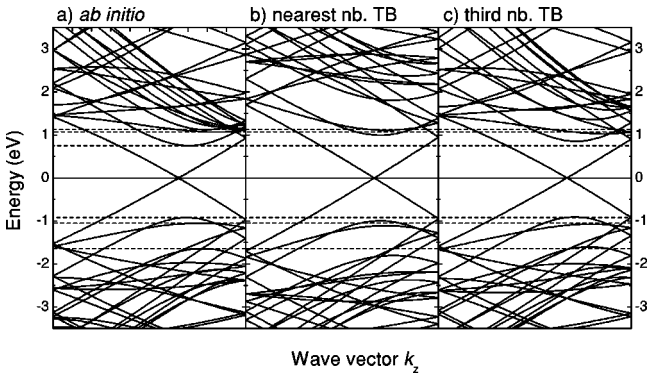

FIG. 6. Band structure of a (12,3) chiral nanotube. (a) *Ab initio* calculation. (b) Nearest-neighbor tight-binding calculation with $\gamma_0 = -2.7$ eV. (c) Third-nearest-neighbor tight-binding calculation with parameters obtained from a fit to the optical energy range; see Table I. The dashed lines denote *ab initio* calculated energies of the singularities in the density of states.

In Figs. 5(a)–5(c) calculations similar to those for the (10,10) tube are shown for the (19,0) zigzag tube with a diameter $d = 1.50$ nm. Again, the agreement between the *ab initio* and third-neighbor tight-binding results is much better than for the nearest-neighbor approximation. As we showed in Ref. 8, the remaining discrepancies between Figs. 5(a) and 5(c) are due to the σ-π hybridization of the curved nanotube wall. Curvature effects are, in general, most pronounced in zigzag nanotubes. Finally, we consider the chiral (12,3) nanotube ($d = 1.30$ nm, $\Theta = 10.9°$). This is an example of a metallic tube with $\mathcal{R} = 3$, i.e., the valence and conduction bands cross at $\approx 2\pi/3a$ in the nanotube Brillouin zone. Figure 6(a) shows the *ab initio* calculations, Fig. 6(b) the next-nearest-neighbor tight-binding band structure, and Fig. 6(c) the third-nearest neighbor tight-binding result. While the valence bands are quite similar in the three approximations, the conduction bands are only poorly described by the nearest-neighbor approximation. The better agreement for the valence band structure can be traced back to Fig. 2(b), where the difference between the *ab initio* calculated band structure for graphene and the nearest-neighbor tight-binding results is smaller for the valence band than for the conduction bands. As for the (19,0) tube, the valence bands of the (12,3) tube are shifted to lower energies in the *ab initio* calculation by curvature effects. Nevertheless, the third-neighbor tight-binding band structure combined with zone folding in Fig. 6(c), which takes only some seconds, already very well describes the first-principles results.

In conclusion, we investigated the tight-binding approximation for the π and π^* bands of graphene. The nearest-neighbor tight-binding dispersion predicts the electronic energies correctly only for a very limited range of wave vectors. If up to third-nearest neighbors are included, the tight-binding approximation quite accurately describes first-principles results over the entire Brillouin zone. The agreement is not restricted to high-symmetry lines, as we demonstrated by combining the tight-binding approximation with a zone-folding approach to calculate the electronic band structure of two achiral and a chiral nanotube.

We acknowledge the Ministerio de Ciéncia y Technología (Spain) and the DAAD (Germany) for travelling support. P. O. was supported by Fundación Ramón Areces, EU Project No. SATURN IST-1999-10593, and Spain-DGI Project No. BFM2000-1312-002-01. J. M. was supported by the Deutsche Forschungsgemeinschaft under Grant No. Th 662/8-1.

[1] T. W. Odom, J.-L. Huang, P. Kim, and C. M. Lieber, J. Phys. Chem. B **104**, 2794 (2000).
[2] A. Jorio, R. Saito, J. H. Hafner, C. M. Lieber, M. Hunter, T. McClure, G. Dresselhaus, and M. S. Dresselhaus, Phys. Rev. Lett. **86**, 1118 (2001).
[3] S. Reich and C. Thomsen, Phys. Rev. B **62**, 4273 (2000).
[4] R. Saito, G. Dresselhaus, and M. S. Dresselhaus, *Physical Properties of Carbon Nanotubes* (Imperial, London, 1998).
[5] C. T. White and J. W. Mintmire, Nature (London) **394**, 29 (1998).
[6] O. Jost, A. A. Gorbunov, W. Pompe, T. Pichler, R. Friedlein, M. Knupfer, M. Reibold, H.-D. Bauer, L. Dunsch, M. S. Golden, and J. Fink, Appl. Phys. Lett. **75**, 2217 (1999).
[7] X. Blase, L. X. Benedict, E. L. Shirley, and S. G. Louie, Phys. Rev. Lett. **72**, 1878 (1994).
[8] S. Reich, C. Thomsen, and P. Ordejón, Phys. Rev. B **65**, 155411 (2002).
[9] A. Kleiner and S. Eggert, Phys. Rev. B **64**, 113402 (2001).
[10] P. R. Wallace, Phys. Rev. **71**, 622 (1947).
[11] D. Sánchez-Portal, P. Ordejón, E. Artacho, and J. M. Soler, Int. J. Quantum Chem. **65**, 453 (1997).
[12] J. M. Soler, E. Artacho, J. D. Gale, A. García, J. Junquera, P. Ordejón, and D. Sánchez-Portal, J. Phys.: Condens. Matter **14**, 2745 (2002); cond-mat/0111138 (unpublished).
[13] N. Troullier and J. L. Martins, Phys. Rev. B **43**, 1993 (1991).
[14] J. P. Perdew and A. Zunger, Phys. Rev. B **23**, 5048 (1981).
[15] H. J. Monkhorst and J. D. Pack, Phys. Rev. B **13**, 5188 (1976).
[16] E. Artacho, D. Sánchez-Portal, P. Ordejón, A. García, and J. Soler, Phys. Status Solidi B **215**, 809 (1999).
[17] J. Junquera, O. Paz, D. Sánchez-Portal, and E. Artacho, Phys. Rev. B **64**, 235111 (2001).
[18] S. Reich, C. Thomsen, and P. Ordejón, Phys. Rev. B **65**, 153407 (2002).
[19] M. C. Schabel and J. L. Martins, Phys. Rev. B **46**, 7185 (1992).
[20] J.-C. Charlier, X. Gonze, and J.-P. Michenaud, Phys. Rev. B **43**, 4579 (1991).
[21] M. Damnjanović, T. Vuković, and I. Milošević, J. Phys. A **33**, 6561 (2000).